Solitary waves in the excitable Burridge-Knopoff model

José Eduardo Morales Morales, Guillaume James, Arnaud Tonnelier

Solitary waves in the excitable Burridge-Knopoff model

J. E. M. Morales, G. James, A. Tonnelier

RESEARCH REPORT
N° 8996
December 2016
Project-Team BIPOP

ISSN 0249-6399 ISRN INRIA/RR--8996--FR+ENG

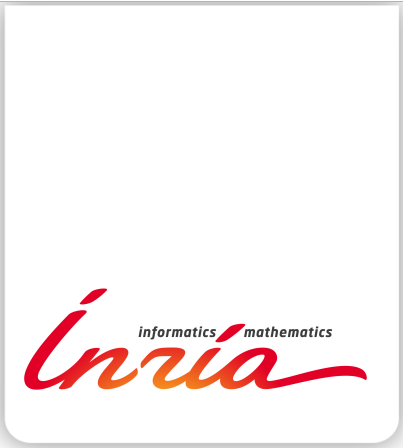

Solitary waves in the excitable Burridge-Knopoff model

J. E. M. Morales, G. James, A. Tonnelier

Project-Team BIPOP

Research Report n° 8996 — December 2016 — 25 pages

Abstract: The Burridge-Knopoff model is a lattice differential equation describing a chain of blocks connected by springs and pulled over a surface. This model was originally introduced to investigate nonlinear effects arising in the dynamics of earthquake faults. One of the main ingredients of the model is a nonlinear velocity-dependent friction force between the blocks and the fixed surface. For some classes of non-monotonic friction forces, the system displays a large response to perturbations above a threshold, which is characteristic of excitable dynamics. Using extensive numerical simulations, we show that this response corresponds to the propagation of a solitary wave for a broad range of friction laws (smooth or nonsmooth) and parameter values. These solitary waves develop shock-like profiles at large coupling (a phenomenon connected with the existence of weak solutions in a formal continuum limit) and propagation failure occurs at low coupling. We introduce a simplified piecewise linear friction law (reminiscent of the McKean nonlinearity for excitable cells) which allows us to obtain analytical expression of solitary waves and study some of their qualitative properties, such as wavespeed and propagation failure. We propose a possible physical realization of this system as a chain of impulsively forced mechanical oscillators. In certain parameter regimes, non-monotonic friction forces can also give rise to bistability between the ground state and limit-cycle oscillations and allow for the propagation of fronts connecting these two stable states.

Key-words: Solitary waves, Burridge-Knopoff model, Excitable media, Lattice dynamical systems.

To be submitted in Wave Motion

RESEARCH CENTRE
GRENOBLE – RHÔNE-ALPES

Inovallée
655 avenue de l'Europe Montbonnot
38334 Saint Ismier Cedex

Ondes solitaires dans le modèle de Burridge-Knopoff excitable.

Résumé : Le modèle de Burridge-Knopoff est un système d'équations différentielles décrivant une chaîne de blocs reliés par des ressorts et tirés sur une surface. Ce modèle a été introduit à l'origine pour étudier les effets non linéaires intervenant dans la dynamique de failles sismiques. L'un des principaux ingrédients du modéle est l'existence d'une force de frottement non linéaire qui dépend de la vitesse entre les blocs et la surface fixe. Pour certaines classes de forces de frottement non monotones, le système présente une réponse importante aux perturbations au-dessus d'un certain seuil; une des caractéristiques des systèmes excitables. A l'aide de simulations numériques, nous montrons que cette réponse est associée à la propagation d'une onde solitaire pour une large gamme de lois de frottement (régulières ou non régulières) et de valeurs de paramètres. Ces ondes solitaires développent des profils de type choc à grand couplage (un phénomène lié à l'existence de solutions faibles dans une limite formelle continue) et un échec de propagation se produit à faible couplage. Nous introduisons une loi de friction simplifiée, linéaire par morceaux (rappelant la non linéarité de McKean pour les cellules excitables), qui nous permet d'obtenir l'expression analytique des ondes solitaires et d'étudier certaines de leurs propriétés qualitatives, telles que la vitesse de l'onde et l'échec de propagation. Nous proposons une réalisation physique possible de ce système comme une chaîne d'oscillateurs mécaniques forcés par impulsion. Dans certains régimes de paramètres, des forces de frottement non monotones peuvent également donner lieu à une bistabilité entre un état stationnaire et un cycle limite et permettre la propagation de fronts reliant ces deux états stables.

Mots-clés : Ondes solitaires, modèle de Burridge-Knopoff, milieux excitables, systèmes dynamiques

1 Introduction

A significant body of work has been devoted to elucidating nonlinear mechanisms of earthquakes [30, 41, 31]. Almost fifty years ago, Burridge and Knopoff [9] introduced a nonlinear lattice model to investigate the generation of earthquakes along faults, or more generally the occurrence of dynamical instabilities at frictional interfaces. The Burridge-Knopoff (BK) model formally describes a chain of blocks connected by springs and pulled over a surface, each block being attached to a spring pulled at constant velocity and subject to a friction force with the surface. When considering two plates under friction, the blocks can either correspond to a discretization of a plate or account for an existing microstructure [27]. It has been shown that this simple slider-block model is able to reproduce some statistical features of earthquakes generated by fault dynamics [12].

A key feature of the BK model lies in the friction force between the blocks and the fixed surface, which depends nonlinearly on sliding velocity. Experiments performed with a broad range of materials have revealed that the steady-state kinetic friction coefficient is non-monotone versus sliding velocity (see [4] for a review). Friction is velocity-strengthening (i.e. frictional resistance increases with sliding velocity) for high enough velocities and becomes velocity-weakening in a regime of low velocities, a behaviour intimately linked with the occurrence of stick-slip instabilities and earthquake phenomena. Such velocity-weakening or velocity-strengthening regimes can be described by different types of friction laws. Rate-and-state friction laws incorporating state variables for the frictional interface are frequently used, see e.g. [36] for a review and a detailed bifurcation analysis in the case of a single block, and [51, 35, 17] for dynamical simulations of the BK model. However, the mathematical analysis of such models can be delicate due to the additional degrees of freedom introduced to describe the state of the interface. Another class of widely used friction laws is given by generalized Coulomb laws with velocity-dependent kinetic friction coefficient [50]. In that case, the set-valued character of the friction laws requires an adapted numerical treatment [1, 6, 53] and leads to analytical complications in dynamical studies [33]. Alternatively, single-valued laws can be used to approximate set-valued friction laws [12] or account for a velocity-strengthening regime at small enough velocities [9, 49, 24].

The dynamics of the BK model has been extensively studied in the case of steady-state velocity-weakening friction. Depending on the choice of parameters and system size, this regime can lead to chaotic dynamics or to the propagation of nonlinear wavetrains [11, 39, 17]. In particular, periodic travelling waves close to solitary waves (with highly localized slipping events propagating at constant velocity) have been reported in numerical and analytical studies [39, 19, 40, 17, 33].

In this paper, we consider a different situation corresponding to 'spinodal' friction laws [9, 20, 36], where steady-state friction is velocity-strengthening both for small and large enough velocities and an intermediate velocity-weakening region exists. This situation has been reported in a number of friction experiments performed with rocks, rubber and hydrogels [43, 52, 24]. In that case, the dynamics of a single block is described by a Van der Pol type equation, a situation frequently encountered in the modelling of excitable media [22, 55, 21, 29]. Numerical studies of the BK model with spinodal friction laws (either generalized Coulomb laws or regularizations thereof) have revealed different types of wave patterns, ranging from synchronous oscillations, periodic travelling waves and phase fronts [14, 13] to chimera-like states (see Fig. 8 of reference [54] for an early observation of this phenomenon). These different studies were focused on the oscillatory regime where the pulling velocity lies within the velocity-weakening region.

With regard to spatially localized travelling waves, the existence of fronts has been established in a continuum limit of the BK model [34] (see also [8, 3, 5] for numerical studies of rupture fronts in other continuum models based on rate-and-state laws). However, the existence of localized

waves was not established so far for the spatially discrete BK model with spinodal friction laws. The analysis of finite amplitude travelling waves in the discrete system is more delicate because it leads to a nonlinear advance-delay differential equation for the wave profiles. In order to tackle this problem, an interesting inverse approach was described in reference [15], where particular friction laws were computed in order to fit prescribed explicit wave profiles. An analytical moving kink solution (with block displacements given by an odd function of the moving frame coordinate z) was proposed but turns out to be erroneous (the velocity dependent friction force induced by the kink is even in z, and cannot be balanced by the odd inertial and stress terms in the dynamical equation (10) of [15]).

In the present paper, we analyse in detail the existence of localized waves in the discrete BK model with spinodal friction laws, using both extensive numerical simulations and analytical techniques. We restrict our attention to solitary waves and will treat the case of fronts in a forthcoming publication. We consider the excitable regime where the pulling velocity lies within a velocity-strengthening domain of the spinodal friction laws (above velocity-weakening). In that case, each single block admits a stable state of continuous slip but displays a large response to perturbations above some threshold. When blocks become coupled, our numerical simulations reveal that this response generates a solitary wave for a broad range of friction laws (smooth or nonsmooth) and parameter values. In the case of regularized Coulomb laws, the solitary wave consists of a moving localized region where sticking occurs, in contrast to the propagation of localized slipping events previously reported for velocity-weakening friction [39].

We analyse in detail the influence of parameters on the existence and qualitative properties of solitary waves. For low enough coupling between blocks, we observe a phenomenon of propagation failure corresponding to the rapid extinction of initially propagating pulses. We find that solitary waves develop shock-like profiles in the opposite limit of large coupling, a phenomenon connected with the existence of weak solutions in a formal continuum limit. When the pulling velocity is decreased towards the boundary of the velocity-strengthening domain, the dynamics of the blocks becomes underdamped and we observe solitary waves with oscillatory tails, while propagation failure takes place above some critical pulling velocity. For certain friction laws (near the transition to a velocity-weakening law), we also observe bistability between continuous slip and limit-cycle oscillations and the existence of propagating fronts connecting these two stable states.

In order to obtain analytical expressions for solitary waves and explain some of their qualitative properties, we introduce a simplified piecewise linear friction law with two velocity-strengthening regions separated by a (negative) jump discontinuity. The discontinuity in the friction force can be interpreted as a rough approximation for the existence of a small intermediate velocity-weakening region. Alternatively, we propose a possible physical realization of this piecewise-linear system as a chain of impulsively forced mechanical oscillators. Such types of nonlinearities have been extensively used for the mathematical study of travelling waves in different types of PDEs [25, 38, 56] and spatially discrete systems [23, 10, 44, 16, 45, 42, 2]. Following this approach allows us to obtain explicit solitary waves in the form of oscillatory integrals and numerically compute their profiles and wave speed. Moreover, this method provides analytical expansions of the solitary waves at small coupling and for pulling velocities near the jump discontinuity [44]. In this limit, we explain the occurrence of propagation failure below some critical coupling by the existence of a saddle-node bifurcation of solitary waves.

It is worthwhile to stress that we obtain fully localized solitary waves, i.e. blocks lie in the state of stable slip at infinity on both sides of the chain (this constitutes another important difference with the previous works [39, 33]). Similar solutions have been previously obtained for other types of excitable lattice dynamical systems where the coupling is diffusive rather than elastic. These systems correspond to spatially discrete FitzHugh-Nagumo equations with either

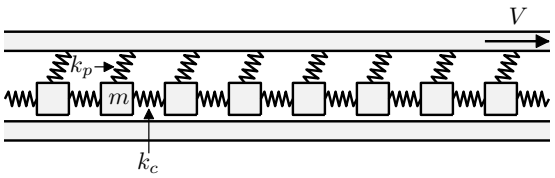

Fig. 1 – The mechanical interpretation of the Burridge-Knopoff model, where V is the pulling velocity or slip rate of the loader plate, m is the mass of a block, k_c and k_p are the stiffness of the Hookean springs.

smooth [28] or piecewise-linear [44] bistable nonlinearities. While our analysis of solitary waves at small coupling closely follows the lines of [44], the properties of solitary waves are quite different at large coupling with the occurrence of shocks in the BK model.

The outline of this paper is as follows. In section 2, we introduce the excitable BK model with different types of spinodal friction laws, summarize several applications of the model (frictional interfaces, mechanical oscillators, nonlinear transmission lines) and illustrate the excitation of solitary waves. In section 3, we use numerical simulations to study the existence and shape of solitary waves depending on parameters. We also consider a continuum limit of the model and illustrate the bistable dynamics near the transition to a velocity weakening law. Section 4 provides analytical results for the idealized piecewise linear friction law. Section 5 summarizes the main findings, describes potential applications of the present work and points out interesting open problems.

2 The Burridge-Knopoff model and its applications

2.1 Dynamical equations and solitary waves

The BK model describes the interaction of two sheared surfaces, one being pulled at a constant speed V and the second is discretized as a chain of N identical blocks with mass m resting over a surface with frictional interaction described by a nonlinear friction function $F(v)$. The blocks are connected to each other through Hookean springs of stiffness k_c, and to the upper plate by springs of stiffness k_p (see Fig. 1).

The motion of an isolated block is given by

$$m\frac{d^2x}{dt^2} + k_p x + f_0 F\left(\frac{V + \frac{dx}{dt}}{v_1}\right) = 0, \tag{1}$$

where $x(t)$ is the displacement of the block relative to the point of attachment on the moving plate, f_0 and v_1 are two scaling parameters of the friction law.

Using the change of variables $y = x/\rho$, $\tau = \rho/v_1$, $\bar{t} = t/\tau$, $\gamma = mv_1^2 k_p/f_0^2$, $\bar{V} = V/v_1$ and $\rho = f_0/k_p$, Eq. (1) can be reformulated as the dimensionless dynamical system on the plane:

$$\begin{aligned} \frac{dy}{dt} &= u, \\ \gamma\frac{du}{dt} &= -F(V+u) - y, \end{aligned} \tag{2}$$

where the rescaled time $\bar{t}$ and pulling velocity $\bar{V}$ have been rewritten as t and V. The qualitative dynamics of (2) highly depends on the shape of the nonlinear function $F(v)$. For a spinodal friction law, similar to the one plotted in Fig. 2A, the system shows excitability: a strong enough

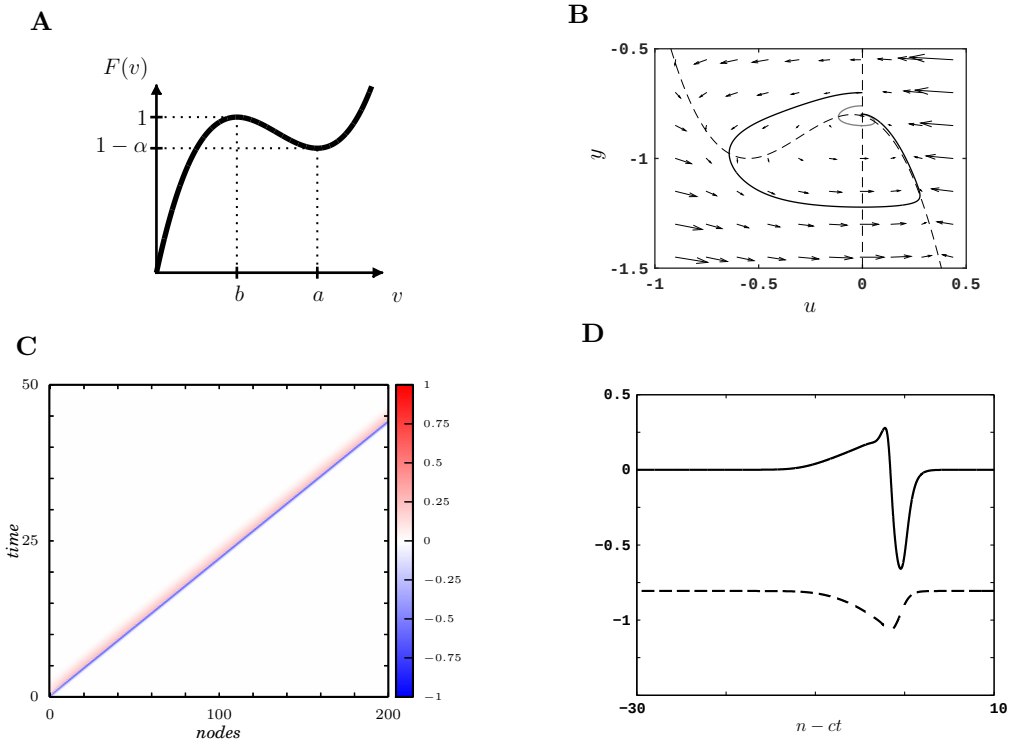

Fig. 2 – **A** The spinodal friction force defined by the cubic polynomial $F_c(v) = 3.2v^3 - 7.2v^2 + 4.8v$ for $v > 0$. In **B**, the responses of an isolated block to perturbations of different magnitudes are shown in the phase plane. The nullclines are represented (dashed lines). For a strong enough perturbation of the resting state, a large trajectory is elicited (solid black), whereas a small perturbation does not produce a significant response (grey line). **C** When the blocks are connected, an initial perturbation of the network elicits the propagation of a stable solitary wave with constant shape and speed. **D** Travelling wave profiles of the velocity (filled line) and the displacement (dashed line) in the moving frame coordinate. Parameters are: $k = 3$, $V = 1.05$, $\gamma = 0.15$. In **B**, the two perturbations are of magnitude 0.11 and 0.05. In **C**, an initial perturbation $(u_0(0), y_0(0)) = (u_s - 1, y_s)$ is imposed on the first block (left edge) of the chain.

perturbation of the steady state $(u_s, y_s) = (0, -F(V))$ produces a large trajectory in the phase plane whereas small perturbations monotonically decay to the resting state. In addition, there exists a refractory period where the block is unresponsive to further perturbations. The geometrical illustration of this threshold effect is shown in Fig. 2B. This excitability property contrasts with the one due to static friction where a critical amount of stress has to be accumulated in order to reach the unstable slipping mode. In our case, for a sufficiently large slip rate V, the slip solution is stable and a temporary incursion in the velocity strengthening creep region is performed following a strong enough perturbation.

When the blocks are interconnected, the resulting network is a discrete excitable medium and the perturbation of one block may propagate to its neighbours producing complex spatiotemporal dynamics, including periodic wave trains, propagating fronts, global oscillations, chaotic dynamics or complex transitions [14, 13]. In the original one-dimensional BK model, the blocks are connected together by springs and the resulting force on the n-th block is given by $k_c \Delta_d x_n$ where $\Delta_d x_n = x_{n+1} - 2x_n + x_{n-1}$ is the discrete Laplacian and k_c is the linear elastic coupling

parameter. Using the dimensionless coupling parameter $k = k_c/k_p$, the governing equations for the n-th block read

$$\begin{aligned} \frac{dy_n}{dt} &= u_n, \\ \gamma\frac{du_n}{dt} &= k\Delta_d y_n - F(V+u_n) - y_n, \end{aligned} \tag{3}$$

where $n \in \mathbb{Z}$.
We report here results on the existence of solitary wave solutions where each block returns to the stable state of continuous slip after wave passage (see Fig. 2C,D). By a solitary wave solution we mean a solution of (3) such that

$$\begin{aligned} u_n(t) &= \varphi(n-ct), \\ y_n(t) &= \psi(n-ct), \end{aligned} \tag{4}$$

with $(\varphi(\pm\infty), \psi(\pm\infty)) = (0, -F(V))$. The function (φ, ψ) defines the waveform, and c is the wave speed that has to be determined. Substitution of (4) into (3) yields the following advance-delay differential equation:

$$\begin{aligned} -c\psi'(\xi) &= \varphi(\xi), \\ -c\gamma\varphi'(\xi) &= k[\psi(\xi+1) - 2\psi(\xi) + \psi(\xi-1)] - F(V+\varphi(\xi)) - \psi(\xi), \end{aligned} \tag{5}$$

where $\xi = n - ct \in \mathbb{R}$ represents the travelling wave coordinate.

The spatiotemporal plot of a solitary wave for the cubic friction law is shown in Fig. 2C and the corresponding waveforms are depicted in Fig. 2D. In the forthcoming sections, we show that the BK model exhibits solitary wave solutions for a large class of nonlinearities F of spinodal type. We also review different physical contexts where such nonlinearities arise.

2.2 Friction dynamics

Several non-monotonic friction laws have been proposed in the context of earthquake fault dynamics. Many studies consider generalized Coulomb friction laws with a multivalued part at the origin (see Fig. 3A,B). This friction law involves a sticking condition when a block achieves a zero velocity with respect to the lower plate. Single-valued regularized Coulomb laws are also often considered for numerical purpose, or to account for the existence of a velocity-strengthening region for low sliding velocities (this can represent e.g. lubrication effects). In addition, friction laws that switch from a velocity-weakening to a velocity-strengthening regime for large sliding velocities are also relevant for applications, see [26] and references therein. Combining these different effects results in spinodal friction laws [14, 13] of the type depicted in Fig. 2A.

In this paper, we investigate the dynamics of the BK model using the prototypical smooth spinodal friction law given by the cubic function $F_c(v) = 3.2v^3 - 7.2v^2 + 4.8v$, depicted in Fig. 2A. We shall denote by $v = a$ the local minimum of the spinodal friction force, the above cubic friction law corresponding to $a = 1$. In order to analyse the effects of a larger class of spinodal friction laws (in particular with different degrees of smoothness or stiffness), we also introduce the following class of piecewise linear functions

$$F_{PL}(v; a, b, \mu) = \begin{cases} \frac{v}{b}, & 0 \le v < b \\ \alpha\left(\frac{v-b}{b-a}\right) + 1, & b < v < a \\ \mu(v-a) + 1 - \alpha, & a < v \end{cases} \tag{6}$$

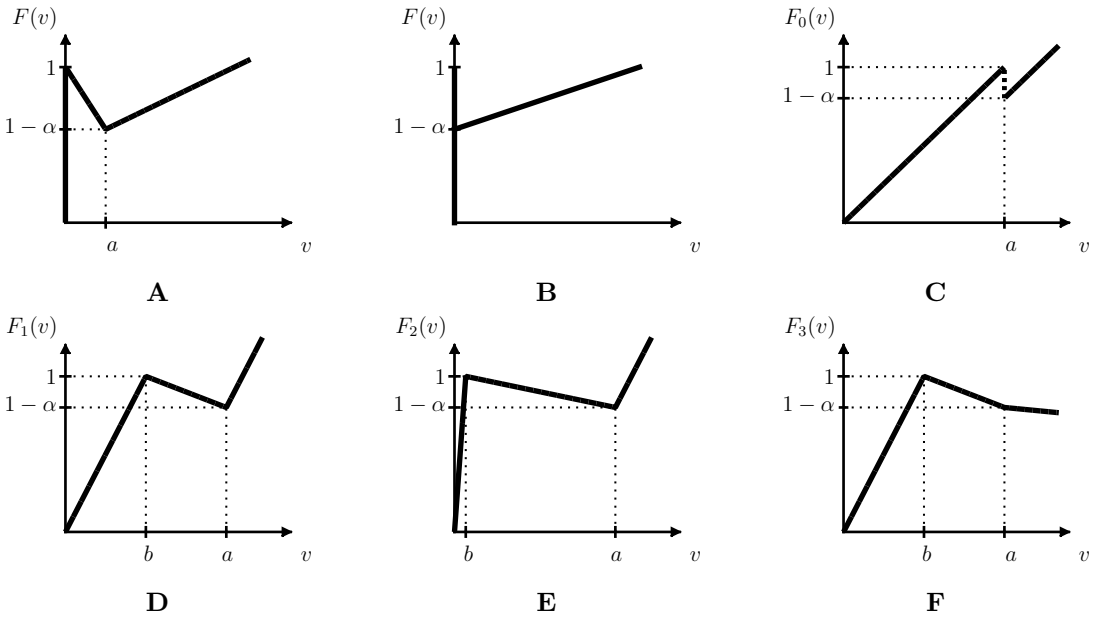

Fig. 3 – Typical piecewise-linear friction laws for the Burridge-Knopoff model. **A**-**E** display different spinodal friction laws (velocity-weakening for an intermediate range of sliding velocities) whereas **F** is velocity-weakening for large enough velocities. **A**, **B** correspond to multivalued laws (generalized Coulomb laws). Velocity-weakening is assumed instantaneous in cases **B**, **C** (the velocity-weakening domains are reduced to a jump discontinuity in the friction force). The single-valued laws **C**-**F** are used in the present work, with $a = 1$ and $\alpha = 0.2$.

that have been normalized so that $F_{PL}(b) = 1$. For $v < 0$ we set $F_{PL}(v) = -F_{PL}(-v)$. The parameter b is the threshold where the transition from velocity strengthening to velocity weakening occurs. If $\mu \geq 0$, velocity strengthening is recovered above the sliding velocity a and $F(a) = 1-\alpha$ ($\alpha \in (0, 1)$) corresponds to a local minimum of the friction force.

We shall consider more specifically four piecewise linear functions defined as follows and depicted in Fig. 3C-F. A crude approximation of spinodal friction laws is given by $F_0(v) = F_{PL}(v; a, a, 1/a)$ (Fig. 3C). In that case, the damping ratio in the two velocity-strengthening regimes are identical and the velocity-weakening region is reduced to a jump discontinuity. This friction function can be rewritten as $F_0(v) = v/a - \alpha H(v - a)$ where H is the Heaviside step function. The friction law defined by $F_1 = F_{PL}(v; a, a/2, 2/a)$ is obtained from F_0 with the addition of an intermediate velocity-weakening region with finite thickness (Fig. 3D). To regularize a multivalued generalized Coulomb law, we also consider $F_2(v) = F_{PL}(v; a, b, 2/a)$ with $b = 0.01$ (Fig. 3E). For this parameter value, the friction law is close to the multivalued case depicted in Fig. 3A. It would be also interesting to investigate the limit case of Fig. 3B (considered e.g. in [34]), but the numerical simulation of the BK model is more delicate in that case and will be investigated in future work. Finally, to investigate the transition from a velocity-strengthening law to a velocity-weakening law at large sliding velocities we introduce $F_3(v) = F_{PL}(v; a, a/2, \mu)$ (Fig. 3F) where the slope μ may be negative.

Note that the present study examines different types of friction laws but is limited to purely linear nearest-neighbours coupling between blocks. Other types of couplings would be relevant

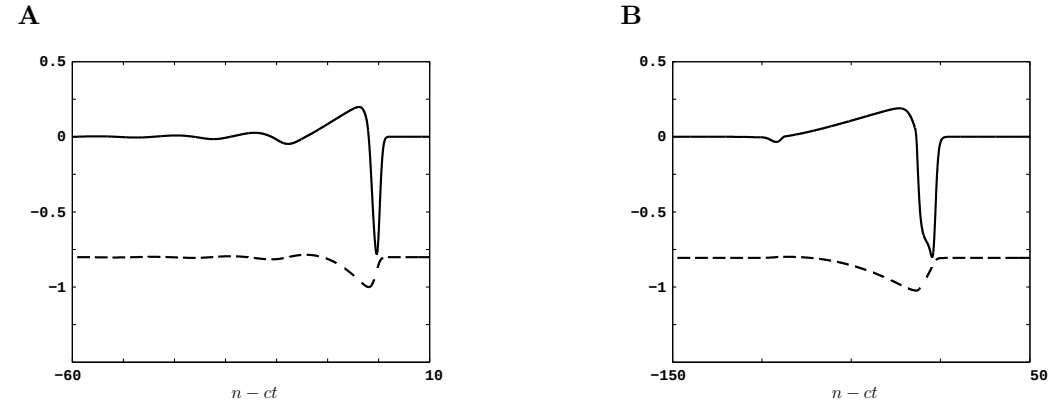

Fig. 4 – Solitary waves profiles $\varphi(n-ct) = u_n(t)$ (solid) and $\psi(n-ct) = y_n(t)$ (dashed) obtained with (**A**) Hertzian and (**B**) linear contact interactions in the Burridge-Knopoff model (cubic friction law). The Hertzian coupling is obtained by replacing the discrete linear Laplacian by $k[(y_{n-1}-y_n)_+^{3/2} - (y_n - y_{n+1})_+^{3/2}]$, and the linear contact law corresponds to $k[(y_{n-1}-y_n)_+ - (y_n - y_{n+1})_+]$, where $(x)_+ = \max(0,x)$. Parameters are: **A**, $k=20$, $V=1.025$ and **B**, $k=150$, $V=1.05$. The wave speeds are **A**, $c \approx 6.36$ and **B**, $c \approx 32.47$, respectively. The wave is generated from the chain at rest except for the last block, where the initial condition is **A** $(u_s - 2, y_s)$ and **B** $(u_s - 1, y_s)$.

for applications, such as long-range elastic couplings or contact interactions (unilateral springs). We have checked that solitary waves can be generated as well in the case of Hertzian interactions or for a linear contact law (see Fig. 4A,B), but a detailed investigation of such systems lies beyond the scope of the present study.

2.3 Oscillator chain with impulsive excitations

In this section we describe a possible physical implementation of the BK model with piecewise-linear friction function F_0 (Fig. 3-**C**). This system corresponds to a chain of coupled linear oscillators, where each element is subject to an impulsive force (applied e.g. using piezo actuators) when reaching a critical deflection $z = \zeta$. The dynamical equations read

$$m\,\ddot{z}_n + \nu\,\dot{z}_n + k_p\,z_n = k_c\,\Delta_d z_n + \lambda \sum_{\substack{t_k \in \mathbb{R},\\ z_n(t_k)=\zeta}} \operatorname{sign}(\dot{z}_n(t_k^-))\,\delta_{t_k}, \tag{7}$$

where $z_n(t)$ is the deflection of the nth oscillator in the chain. In the right side of (7), δ_{t_k} denotes the Dirac distribution at $t = t_k$, *sign* the usual sign function (odd and equal to unity on $(0,+\infty)$), and we use the notation $\dot{z}_n(t_k^-)$ (resp. $\dot{z}_n(t_k^+)$) for the left (resp. right) limit of $\dot{z}_n$ at $t = t_k$. For the series of impulses to be well defined as a distribution, it is assumed that each component $z_n(t)$ crosses the critical value $z = \zeta$ for a countable set of times t_k (generally depending on n) without finite accumulation point (i.e. Zeno behaviour does not occur). The external (state-dependent) impulsion has a fixed magnitude $\lambda > 0$ and is always applied in the direction of motion. Each oscillator is damped ($\nu > 0$ denotes the associated damping constant) and the other physical parameters in (7) are the same as in section 2.1.

The components z_n correspond to continuous piecewise-differentiable functions, displaying jumps of derivatives at $t = t_k$. One obtains from (7)

$$[\dot{z}_n]_{t_k} = \frac{\lambda}{m} \operatorname{sign}(\dot{z}_n(t_k^-)), \tag{8}$$

with $[f]_{t_0} = f(t_0^+) - f(t_0^-)$ denoting the jump discontinuity of a function f at t_0. In order to map (7) to the piecewise-linear BK model, we need the following technical lemma.

Lemma 1. *Let u denote a continuous piecewise-differentiable function such that $u(0) = 0$, $\dot{u}(0^-) \neq 0$. The following properties are equivalent :*

$$\begin{aligned} &i) \quad \operatorname{sign}([\dot{u}]_0) = \operatorname{sign}(\dot{u}(0^-)), \\ &ii) \quad \operatorname{sign}([\dot{u}]_0) = [H(u)]_0. \end{aligned}$$

Proof. Let us first assume *i)* and show that *ii)* holds true. Since $\dot{u}(0^+) = \dot{u}(0^-) + [\dot{u}]_0$, *i)* implies $\operatorname{sign}(\dot{u}(0^+)) = \operatorname{sign}(\dot{u}(0^-))$. This equality implies $[H(u)]_0 = \operatorname{sign}(\dot{u}(0^\pm))$ (since $\dot{u}(0^\pm) \neq 0$), which leads to *ii)* using *i)*.

Now let us show that *ii)* implies *i)*. We prove this statement for $\dot{u}(0^-) > 0$, the proof for $\dot{u}(0^-) < 0$ being similar. The above assumptions imply $\operatorname{sign}([\dot{u}]_0) = [H(u)]_0 \geq 0$, hence $\dot{u}(0^+) \geq \dot{u}(0^-) > 0$, leading to $[H(u)]_0 = 1$. From *ii)* we then get $\operatorname{sign}([\dot{u}]_0) = 1$ and thus *i)* holds true. □

In the sequel we restrict our attention to solutions of (7) satisfying the following transversality condition for all n and all crossing times t_k :

$$\dot{z}_n(t_k^-) \neq 0. \tag{9}$$

Applying lemma 1 to $u(t) = z_n(t + t_k) - \zeta$, property *i)* is satisfied thanks to (8) (with $\lambda, m > 0$) and thus $\operatorname{sign}(\dot{u}(0^-)) = [H(u)]_0$, meaning that

$$\operatorname{sign}(\dot{z}_n(t_k^-)) = [H(z_n - \zeta)]_{t_k}. \tag{10}$$

Consequently, equation (7) and the transversality condition (9) lead to

$$m\,\ddot{z}_n + \nu\,\dot{z}_n + k_p\,z_n = k_c\,\Delta_d z_n + \lambda\,\frac{d}{dt}\,H(z_n - \zeta). \tag{11}$$

Similarly, applying lemma 1-*ii)* to any solution of (11) satisfying (9), one establishes the equivalence between equations (7) and (11) under the above transversality condition.

Assuming further $z_n(0) \neq \zeta$ for all n and integrating (11) on $[0, t]$, one obtains the equivalent formulation

$$m\,\dot{z}_n + \nu\,(z_n - \zeta - \frac{\lambda}{\nu}\,H(z_n - \zeta)) = (k_c\,\Delta_d - k_p)\,\int_0^t z_n(s)\,ds + p_n \tag{12}$$

with

$$p_n = m\,\dot{z}_n(0) + \nu(z_n(0) - \zeta) - \lambda\,H(z_n(0) - \zeta).$$

Let us either consider an infinite lattice with periodic or free end boundary conditions, or bounded sequences $(z_n, \dot{z}_n)$ on an infinite lattice. In each case the linear map $k_c\,\Delta_d - k_p$ is invertible ($k_c, k_p > 0$) and one can introduce the new variable

$$x_n(t) = \int_0^t z_n(s)\,ds + (k_c\,\Delta_d - k_p)^{-1} p_n - \frac{f_0}{k_p},$$

where f_0 denotes an arbitrary constant. Substitution in (12) leads to the piecewise-linear BK model

$$m\,\ddot{x}_n + F(\dot{x}_n) + k_p\,x_n = k_c\,\Delta_d x_n, \tag{13}$$

where

$$F(u) = \nu\,(u - \zeta) - \lambda\,H(u - \zeta) + f_0. \tag{14}$$

This family of piecewise-linear functions is parametrized by the slope ν, position ζ and magnitude λ of the jump discontinuity and local maximum f_0.

2.4 Nonlinear transmission lines

The mechanical BK system (3) has an electrical equivalent as an active transmission line made of electronic L-C circuits coupled to a diode. The corresponding two-node circuit has been already

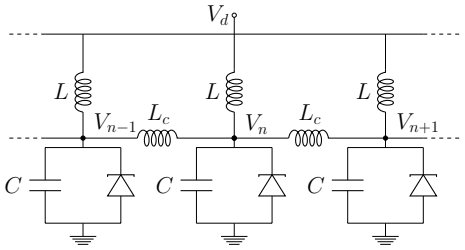

Fig. 5 – Electrical analogue of the excitable Burridge-Knopoff model as a nonlinear transmission line.

introduced and studied [48].
Application of Kirchoff's current law at the node n (see Fig. 5) gives

$$C\frac{d^2Y_n}{dt^2} + \left(\frac{1}{L} + \frac{1}{L_c}\right) Y_n - \frac{1}{L_c}\left(Y_{n+1} + Y_{n-1}\right) + F\left(V_d + \frac{dY_n}{dt}\right) = 0, \tag{15}$$

where $Y_n = \int (V_n - V_d)$, V_n is the voltage at node n, V_d is the driving voltage, C is the capacitance, L and L_c are inductances, and the function F defines the current-voltage relationship of the nonlinear component. For $L = L_c/(1 + L_c)$, $C = \gamma$, $k = 1/L_c$, $y_n(t) = Y_n(t)$ we recover the BK system (3). The tunnel diode has a spinodal current-voltage characteristic as the one depicted in Fig. 2A (in the I-V plane) where a negative resistance occurs at intermediate voltage values. A sufficiently strong voltage perturbation may initiate the propagation of a solitary wave along the transmission line. Potential applications of nonlinear electrical wave propagation in electronic devices include broadband circuits, microwaves, instrumentation and the electronic generation of optical signals [37].

3 Qualitative properties of solitary waves

3.1 Regimes of solitary wave generation

Unless stated otherwise, simulations are done with a network size and for a time duration such that a stationary solution is reached. The network is initialized at its resting state $(u_s, y_s)_n$ and free boundary conditions are taken. For the numerical integration, the adaptive scheme Lsoda is employed with a minimal error tolerance set at $1.5e{-}8$. A time step $\Delta t = 0.001$ is used to follow the numerical solution. All the numerical results are illustrated with the fixed parameter $\gamma = 0.15$ that sets the simulations in the overdamped regime. The underdamped case will be briefly discussed. The existence of solitary waves is explored in the excitable regime, i.e. for a pulling velocity such that $a < V < V_{max}$, where $V_{\max} > a$ is defined through $F(V_{\max}) = 1$. The two limiting regimes, $V \to a^+$ and $V \to V_{max}^-$, will be referred to as the small pulling velocity regime and the maximal pulling velocity regime, respectively. To explore intermediate velocity regimes, we also consider a medium pulling velocity $V_{med} > a$ defined through $F(V_{med}) = 1{-}\alpha/2$. For ensuring a stable localized wave propagation, typical network size is of order one hundred for small pulling velocities, whereas medium velocities require around ten thousands blocks. Such

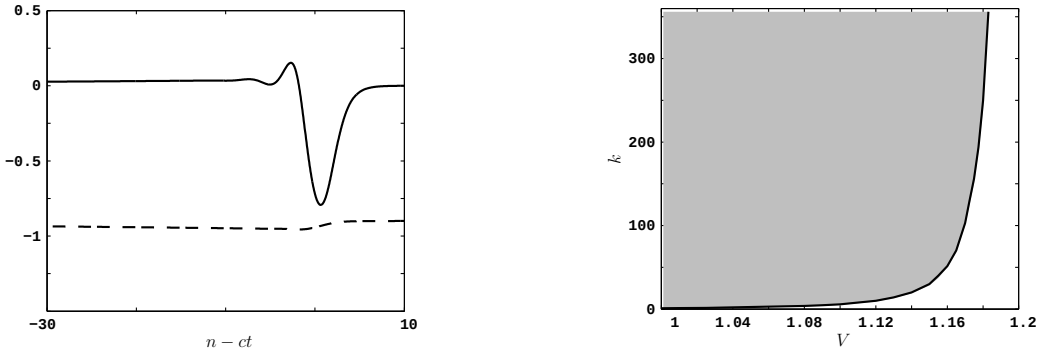

A **B**

Fig. 6 – **A** Wave profiles of the velocity $\varphi(n-ct)$ (solid) and the displacement $\psi(n-ct)$ (dashed) for the cubic friction law $F_c(v)$, $V = 1.183$ and $k = 400$. The wave speed of the localized travelling wave is $c \approx 50.05$. **B** Regimes of existence and stability of solitary waves in the $V - k$ plane (grey shading) for the cubic friction law. The solid line indicates the critical coupling values k^* below which propagation failure occurs. Regimes are computed from numerical simulations in which the wave is initiated by imprinting a velocity u_p to the first block in the chain (magnitude up to $u_p = -10$). Note that here $V_{\max} = 1.25$.

large network simulations have to be performed because the increase of V also requires increasing k in order to excite solitary waves (see below). This parameter regime results in higher wave speed, convergence time towards steady state, and pulse width (simulations for these network sizes can be efficiently addressed using Python programming language).

Propagating waves are initiated using a shock-like initial condition: a strong perturbation is applied on the resting state of a subset of blocks in the network, possibly reduced to a single block perturbation near the left edge of the network. The shock excitation is applied to the position or to the velocity. The magnitude of the excitation required to generate a propagation depends on V. In the regime of small pulling velocity, a velocity perturbation of magnitude in the interval $[0.125, 2.5]$ is sufficient to excite a solitary wave for all friction forces. An excitation of the position is more efficient to produce trains of solitary waves and a perturbation magnitude in the interval $[0.01, 0.5]$ is used (this higher sensitivity to perturbations of positions is clearly illustrated for a single block by Fig. 2-B). For a medium pulling velocity ($V \sim V_{med}$), a stronger perturbation on the velocity is needed, up to 10, whereas perturbations in the position remain similar. In the maximal velocity regime, excitations of the network fail to produce travelling waves.
Localized solutions can propagate stably along the network in the excitable regime for a sufficiently large coupling value. The wave speed and width increase with the coupling value when the other parameters are fixed, while the increase of γ decreases the wave speed. For a given pulling velocity, there exists a critical coupling value k^* below which no propagation occurs. This phenomenon has been coined propagation failure and is well documented for excitable lattices of diffusive type [32]. As V increases, the critical value k^* increases and a vertical asymptote is observed near $V = V_{max}$. This is shown in Fig. 6B where the regime of existence and stability of solitary waves is indicated in the $V - k$ plane for the cubic friction law. Qualitatively similar results are obtained for the other spinodal friction functions (results not shown). Table 1 presents computations of k^* values for different friction laws and pulling velocities.

Friction function	Small pulling velocity $V = 1.025$	Medium pulling velocity V_{med}
$F_c(v)$	$k^* \approx 1.4$	$k^* \approx 360.8$
$F_0(v)$	$k^* \approx 0.43$	$k^* \approx 1915.3$
$F_1(v)$	$k^* \approx 4.5$	$k^* \approx 99$
$F_2(v)$	$k^* \approx 48$	$k^* \approx 602$

Table 1 – Critical coupling k^* for different friction functions and different pulling velocities. Parameter values for a, b and α are as in Fig. 3.

The increase of k^* versus V can be intuitively explained by the geometry of excitability of a single block: for small pulling velocities, the initial state of the network is near the right knee of the spinodal friction function and a small perturbation is sufficient to reach the threshold of excitability. As V increases, the steady state gets away from the threshold separatrix and the perturbation has to be stronger in order to initiate a large response of the block. Above V_{max} the excitability property of the block disappears.
The waveforms obtained for different friction laws, pulling velocities V and coupling strengths k share common features. The displacement profile presents a hump whereas the velocity profile shows a rapid downstroke followed by an upstroke reminiscent to the action potential of spiking neurons. This is illustrated in Fig. 7A-D using the different friction laws. Note that $\int_{\mathbb{R}} \varphi \, d\xi = c\,(\psi(+\infty) - \psi(-\infty)) = 0$. Moreover, the discontinuous law defined by F_0 produces a rather symmetric velocity profile where the positive and negative peaks are quasi-equidistant from the resting state. This property is more pronounced in the small pulling velocity regime and tends to break down as V increases. This symmetry is broken for the other friction laws (F_c, F_1, F_2 and F_3) where the positive peak of the velocity profile is less marked. When the velocity weakening range increases, the amplitude of the negative peak of the velocity profile becomes larger while the wave speed decreases.
The tail of the velocity profile presents either a monotonic or an oscillatory return to the resting state. This feature is determined by the modes around the resting state. Linearisation of (3) around the steady state $(u_n, y_n) = (0, -F(V))$ reads

$$\gamma \ddot{y}_n = k\Delta y_n - y_n - F'(V)\dot{y}_n. \tag{16}$$

In order to analyse the relaxation towards the rest state, we look for normal modes $y_n(t) = Ae^{iqn+\sigma(q)t} + c.c.$ where $A \neq 0$ and $\sigma(q)$ are two complex numbers, $q \in [0, \pi]$ and c.c. stands for complex conjugate. This leads to

$$\sigma(q) = \left[-F'(V) \pm \sqrt{\Delta(q)}\right] \frac{1}{2\gamma}, \tag{17}$$

where $\Delta(q) = F'(V)^2 - 4\gamma\left[1 + 4k\sin^2(q/2)\right]$ is a decreasing function of q on $[0, \pi]$. The asymptotic decay rate is controlled by the slowest decaying mode (obtained for $q = 0$), which also describes the relaxation of the uncoupled system. When V approaches the local minimum of the cubic friction force F_c, the value of $F_c'(V)$ tends towards 0 and all modes become underdamped (σ being imaginary). The resulting feature is an oscillatory tail of the wave as shown in Fig. 7D where the envelope of the oscillations becomes larger as V decreases. Due to the constant derivative of the piecewise linear friction forces F_0, F_1, F_2 for sliding velocities above a, the modes do not depends on V. In that case the occurrence of oscillatory behaviour can be analysed as above and only depends on γ, k and the slope μ in (6).
In the following two subsections we explore two limiting regimes of particular interest: the continuum limit and a bistability regime.

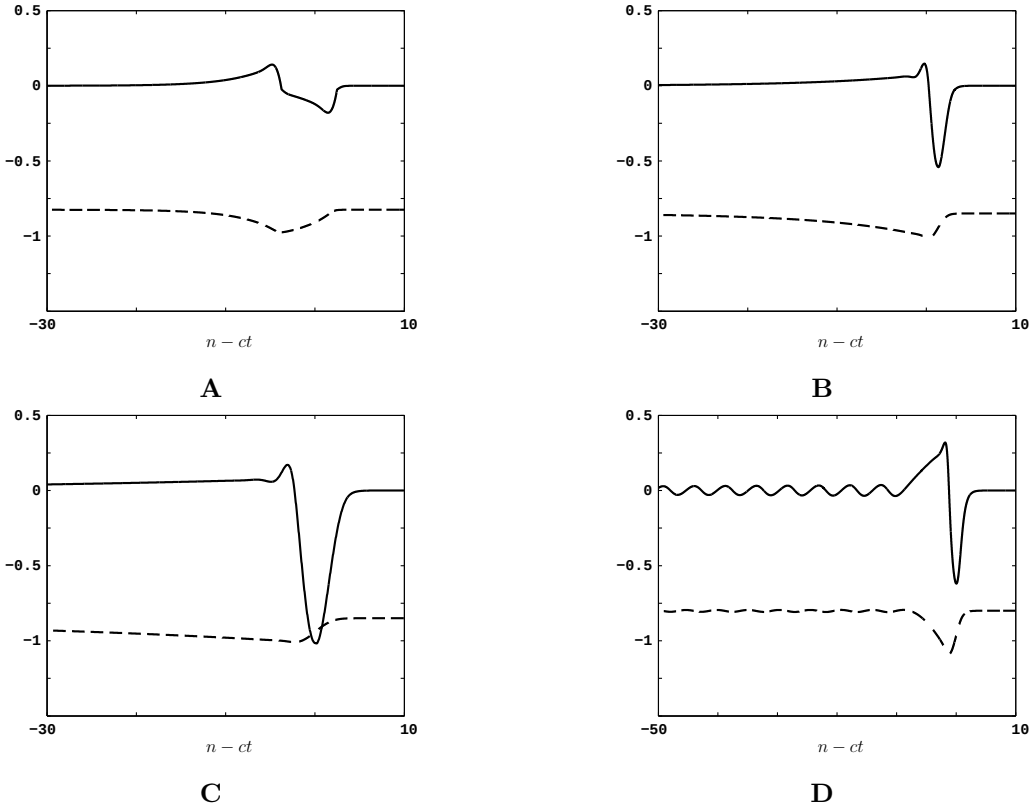

Fig. 7 – Plot of the waveforms $\varphi(n-ct)$ (solid) and $\psi(n-ct)$ (dashed) for, **A** $F_0(v)$, $V=1.025$, $k=2$, **B** $F_1(v)$, $V=1.025$, $k=5$, **C** $F_2(v)$, $V=1.025$, $k=70$ and, **D** $F_c(v)$, $V=1$, $k=2$. The local minimum of each spinodal friction force is located at $a=1$. The computed wave speed values are $c=4.39$, $c=5.36$, $c=21.23$, $c=4.04$ for **A-D**, respectively. Simulations are done for a strong perturbation ($u_p=-10$) of the velocity of the first block.

3.2 Continuum limit

We are interested in the study of solitary waves when the discrete BK model approaches a continuum limit, i.e. for $k \gg 1$. Near the continuum limit, system (3) takes the form:

$$\gamma\frac{\partial^2 y}{\partial t^2}+F\left(V+\frac{\partial y}{\partial t}\right)+y=\frac{\partial^2 y}{\partial x^2}+\frac{h^2}{12}\frac{\partial^4 y}{\partial x^4}+\mathcal{O}(h^4) \tag{18}$$

where we have set $y_n(t)=y(x,t)$, $x=n/\sqrt{k}$ and $h=1/\sqrt{k}\ll 1$. Equation (18) is the so-called Boussinesq approximation. We look for solitary wave solutions of (18) and set $y(x,t)=Y(s)$ with $s=x/\tilde{c}-t$ (for system (3), this corresponds to solitary waves with large velocity $c=\tilde{c}\sqrt{k}$). The above Ansatz leads to the ODE

$$\Lambda Y''-F\left(V-Y'\right)-Y=-\frac{h^2}{12\tilde{c}^4}Y^{(4)}+\mathcal{O}(h^4) \tag{19}$$

where $\Lambda=1/\tilde{c}^2-\gamma$.

The fourth derivative at the right side of (19) may be useful to account for the appearance of high frequency oscillations (see below), but this problem will not be analysed in the present

study. In this work we restrict to the second order model obtained by neglecting $\mathcal{O}(h^2)$ terms, which reads

$$\Lambda Y''(s) - F\left(V - Y'(s)\right) - Y = 0. \tag{20}$$

This equation admits the unique equilibrium $(Y, Y') = (-F(V), 0)$. In what follows we study the case of the cubic friction law $F = F_c$. The equilibrium point is a saddle point for $\Lambda > 0$, an unstable point (source) for $\Lambda < 0$ and $\Delta \geq 0$, an unstable focus for $\Lambda < 0$ and $\Delta < 0$, where $\Delta = F'(V)^2 + 4\Lambda$. The existence of a smooth solitary wave corresponds to the existence of an homoclinic orbit for equation (20). In the unstable configuration ($\Lambda < 0$) it is clear that such an orbit cannot exist. In the saddle case ($\Lambda > 0$), an additional equilibrium inside the homoclinic orbit has to be present because the phase space is two-dimensional. Since there is only one single equilibrium point, smooth solitary waves cannot exist in the continuum model (20).

However for large k values, numerical simulations of the discrete BK model reveal the existence of solitary waves. Typical profiles of these waves are shown in Fig. 8. The velocity component displays two shocks (resulting in two slope discontinuities for the displacement component), and we observe long-lived (i.e. metastable) oscillations in the vicinity of the rear shock. An interesting open question concerns the existence of exact travelling wave solutions of this type (i.e. with an oscillatory shock) in the BK model (3) or in the higher order continuum model obtained by neglecting $\mathcal{O}(h^4)$ terms in (19). These problems will be addressed in future works using numerical continuation techniques. After a very long transient, the fast oscillations near the rear shock disappear, which leads to the shock-wave profiles displayed in the right column of Fig. 8. Given the long time scale of simulations, it is not clear whether this slow drift towards a non-oscillatory shock is a dynamical property of the BK model or is due to numerical integration errors.

The profile of the asymptotic non-oscillatory pulse can be analytically captured by considering equation (20) with $\Lambda = 0$, which corresponds to fixing $\tilde{c} = \sqrt{1/\gamma}$. In that case, the solitary wave of (3) propagates at the sound velocity $c = \sqrt{k/\gamma}$. This case leads to the differential-algebraic equation

$$Y = -F(V - Y'). \tag{21}$$

Solutions of (21) are plotted in Fig. 8 (blue lines). They correspond to weak solutions $y(x,t) = Y\left(x/\tilde{c} - t\right)$ of the nonlinear PDE obtained by setting $h = 0$ in (18). In particular, the solution of (21) shown the right column of Fig. 8 perfectly matches the stationary profiles shown in Fig. 8C,E. For the parameter values provided in Fig. 8, the wave speed of the numerically observed solitary wave is $c \approx 2587$ and the analytical approximation $c = \sqrt{k/\gamma} = 2582$ is quite accurate (relative error $< 2.10^{-3}$). In the case of oscillatory shocks, solutions of (21) provide reasonably accurate approximations of block displacements (see Fig. 8D), but they only approximate velocity oscillations on average near the rear shock (Fig. 8B).

3.3 Bistability regime

The excitable nature of system (3) can give rise to an oscillatory behaviour, similar to the self-sustained oscillations produced by excitable membranes in biology [18]. The state of continuous slip loses its stability when the friction law operates a transition from a velocity-strengthening regime to a velocity-weakening regime. For the friction law F_3 defined in section 2.2, this case occurs when $V > a$ and the slope parameter μ switches from positive to negative. The dynamics of a single block is illustrated in the top panels of Fig. 9. In the velocity-weakening regime $\mu < 0$, there exists a large-amplitude stable limit cycle, which persists in the range $\mu > 0$ provided μ is not too large (see the bifurcation diagram in Fig. 9A). For the state of continuous slip, a subcritical Hopf bifurcation occurs at $\mu = 0$, leading to the existence of an unstable

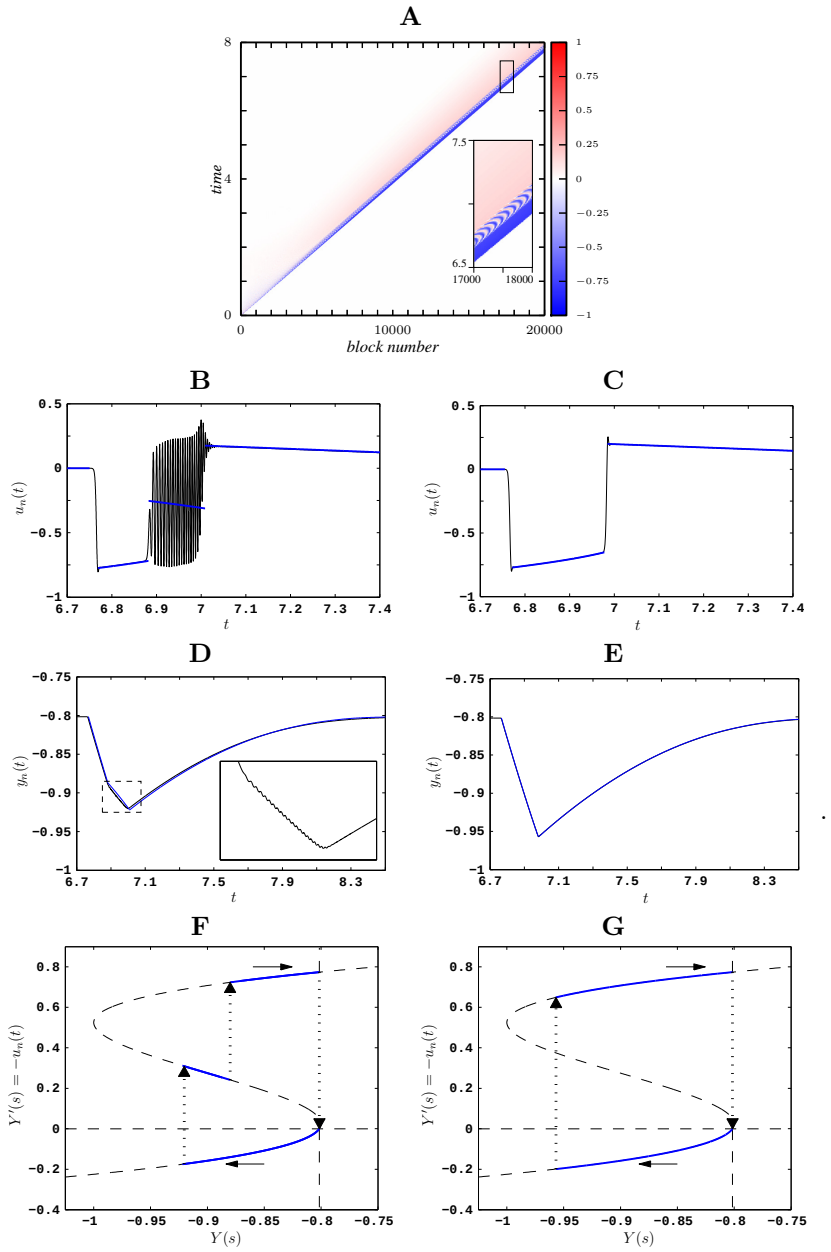

Fig. 8 – Simulation of the BK model (3) in the high coupling limit ($k = 10^6$), for $V = 1.025$ and friction law $F_c(v)$. **A** Spatiotemporal plot of $u_n(t)$. When the pulse reaches $n > 15000$, a quasi-stationary state is reached. **B** Plot of $u_n(t)$ (black line) for $n = 17500$ and **D**, plot of $y_n(t)$ (black line) where the inset is an enlargement that shows the small fluctuations of $y_n(t)$ in the highly oscillatory region of $u_n(t)$. In **C** and **E**, we plot the asymptotic solitary wave profiles for $n > 95000$ (time has been shifted for convenience). In **F** and **G**, the blue lines are different solutions of (21) that match the quasi-stationary waveforms shown in **B,C** and **D,E**, respectively. Nullclines of (20) are represented in the (Y, Y') plane as dashed lines. Solid arrows indicate the time trajectory. Dotted arrows represent the fast transition between the blue lines of plots **B** and **C**. Initial excitation: $(u_0(0), y_0(0)) = (u_s - 10, y_s)$.

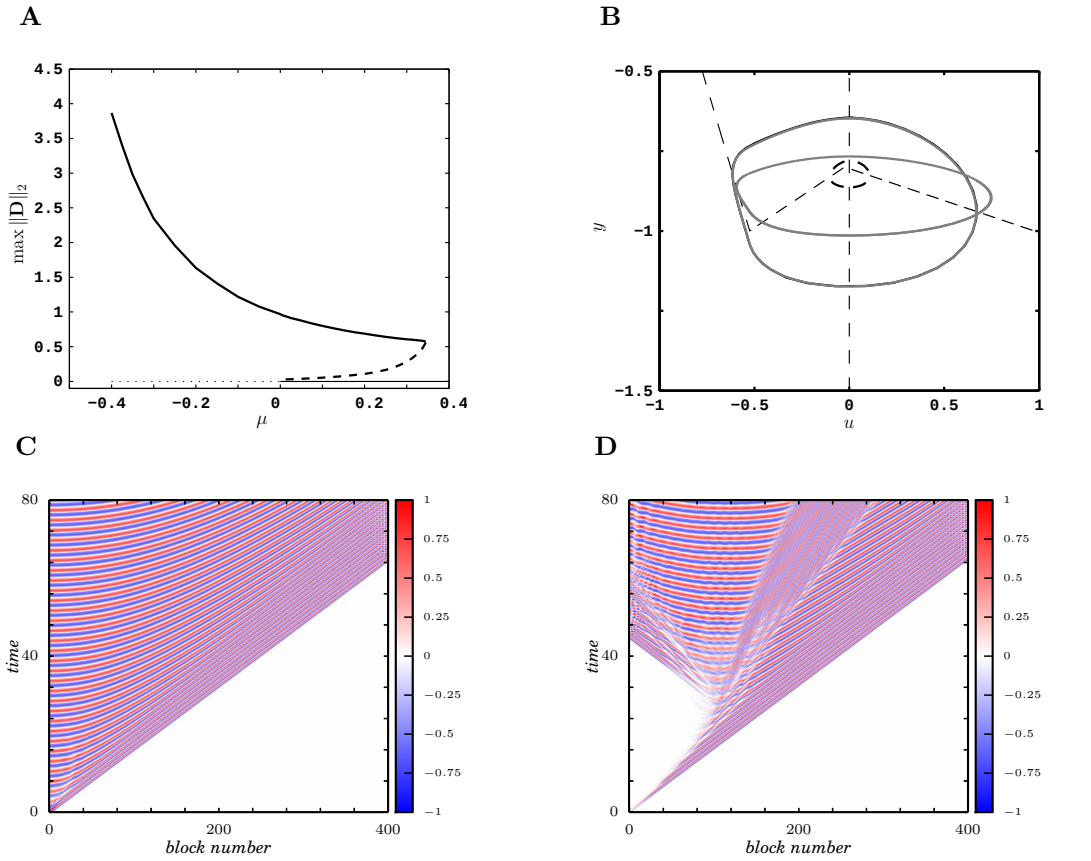

Fig. 9 – Simulations of the BK model with friction law $F_3(v)$ in a bistable regime, with $\mu = 0.2$, $V = 1.025$ and $k = 5$. **A** Bifurcation diagram of a single block that shows the amplitudes of the stable (solid line) and unstable (dashed line) periodic orbits. The amplitude is defined by $\max_{t>0} \|(u(t) - u_s, y(t) - y_s)\|_2$, where (u_s, y_s) is the equilibrium state. The latter is stable (solid straight line) or unstable (dotted straight line) depending on μ. **B** Phase plane of a single block. The nullclines (dashed lines), the stable limit cycle (bold solid circle) and unstable limit cycle (dashed line) are represented. **C,D** Wave patterns generated in the chain of blocks. A perturbation $(u_0(0), y_0(0)) = (u_s + u_p, y_s)$ with $u_p = -10$ is used in **C**, whereas $u_p = -0.25$ is used in **D**. For the simulation shown in **C**, the asymptotic states of two blocks ($n = 0$, $n = 380$) are also plotted in figure **B**, where the trajectory of the first block converges towards the limit cycle.

periodic orbit when μ is positive and not too large. If μ further increases, the two periodic orbits disappear through a saddle-node bifurcation. Consequently, there exists a narrow interval of positive values of μ where the model exhibits bistability between the state of continuous slip and a limit cycle (a typical phase portrait is shown in Fig. 9B). The two attractors are separated by an unstable periodic orbit, and a change of position (or velocity) can switch the system from rest to oscillation and vice versa.

In this parameter regime, it is an interesting problem to examine the possible spatiotemporal patterns which can be generated by coupling the bistable units. The stability of steady sliding can be analysed through the linear system (16), with eigenvalues given by (17) for $F'(V) = \mu$. For $\mu > 0$, the equilibrium state (u_s, y_s) is locally asymptotically stable, while for $\mu < 0$ it

becomes unstable. For $\mu > 0$, different types of dynamics can be observed depending on the initial perturbation, as exemplified by Fig. 9C-D. In this example, velocity perturbations of one block with large magnitudes produce a front wave with oscillations in the back (periodic travelling waves are clearly visible), while much smaller perturbations produce complex oscillatory patterns. The dynamics of the BK model in the bistable regime is likely to be very rich and needs to be explored in more detail in future works.

4 Construction of solitary waves for the discontinuous piecewise-linear friction force

In this section we study analytically and numerically the solutions of the following travelling wave equation derived from (5):

$$c^2\gamma \frac{d^2\varphi}{d\xi^2} = k\Delta_d\varphi + c\frac{d}{d\xi}F(V+\varphi) - \varphi, \tag{22}$$

with $\varphi(\xi) \to 0$ as $\xi \to \pm\infty$. We consider the friction force given by the piecewise linear function:

$$F_0(v) \quad = \quad \frac{v}{a} - \alpha H(v-a), \quad v > 0,$$

where the velocity weakening regime is assumed to be instantaneous. A strict velocity threshold occurs at the discontinuity $\varphi = -\beta = a - V < 0$ unlike the smooth velocity threshold induced by the cubic friction law. Numerical simulations suggest that this piecewise linear model captures the qualitative features of the localized solitary waves observed for a broader class of friction forces.
The strict velocity threshold makes it possible to classify travelling waves based on the threshold hitting. Let us define the decreasing (finite or infinite) sequence $(\xi_k)_k$ through

$$\varphi(\xi_k) \quad = \quad -\beta.$$

Translation invariance of the solution allows us to fix $\xi_0 = 0$. Different wave types can be obtained according to their signature $(\sigma_j)_j$ defined as (see Fig. 10)

$$\sigma_j \quad = \quad [H(\varphi+\beta)]_{\xi_j}.$$

We distinguish between threshold crossing from above, threshold crossing from below, and threshold reaching without crossing that read $\sigma_j = -1$, $\sigma_j = 1$, and $\sigma_j = 0$, respectively. The solitary wave solutions are classified according to the changes of sign of $\varphi+\beta$ that is given by the sequence $(\sigma_j)_j$. It is worth nothing that travelling sliding solutions are excluded, i.e. the solution is not allowed to remain on the discontinuity line of the friction force.
Fixing $(\sigma_j)_j$, we have:

$$\begin{aligned}
\frac{d}{d\xi}F_0(V+\varphi) &= \left\{\frac{d}{d\xi}F_0(a+\varphi+\beta)\right\} + \sum_i [\,F_0(a+\varphi+\beta)\,]_{\xi_i}\,\delta_{\xi_i}, \\
&= \{F_0'(a+\varphi+\beta)\}\,\{\varphi'\} + [F_0]_a \sum_i \sigma_i\,\delta_{\xi_i}, \\
&= \frac{\varphi'}{a} - \alpha\sum_i \sigma_i\,\delta_{\xi_i},
\end{aligned}$$

where δ_{ξ_i} is the Dirac distribution at ξ_i. Travelling waves in the class $(\sigma_j)_j$ satisfy the linear non-homogeneous differential equation:

$$c^2\,\gamma\,\varphi'' - \frac{c}{a}\,\varphi' + \varphi \quad = \quad k\,\Delta_d\varphi - c\,\alpha\,\sum_i \sigma_i\,\delta_{\xi_i}. \tag{23}$$

A solution of (23) is a travelling wave solution of (22) if the crossing conditions at $(\xi_j)_j$ are satisfied together with the sign conditions given by the signature $(\sigma_j)_j$. This leads to the following admissibility conditions:

$$\left\{\begin{array}{l} \varphi(\xi_{2j}) = \varphi(\xi_{2j+1}) = -\beta \\ \varphi(\xi) < -\beta \ \text{ if } \ \xi \in]\xi_{2j+1}, \xi_{2j}[\\ \varphi(\xi) > -\beta \quad \text{otherwise,} \end{array}\right. \tag{24}$$

where we assume for clarity that there is no threshold reaching without crossing (no i such that $\sigma_i = 0$).

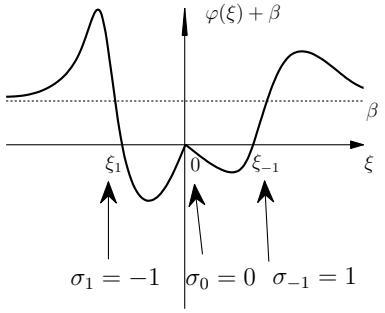

Fig. 10 – Signature $(\sigma_j)_j$ for the different threshold crossings.

By Fourier transform, we construct a localized solution $\varphi(\xi)$ of system (23). A travelling wave solution can be expressed as

$$\varphi(\xi) \quad = \quad \sum_p \int_{\mathbb{R}} e^{i2\pi\lambda\xi} g_{c,\xi_p}(\lambda) d\lambda \tag{25}$$

where

$$g_{c,\xi_p}(\lambda) \quad = \quad \alpha c \sigma_p e^{-2\pi i\lambda\xi_p} \left[4\pi^2 c^2\lambda^2\gamma - 4k\sin^2(\pi\lambda) + \frac{2\pi i c\lambda}{a} - 1\right]^{-1}.$$

The analytical expression (25) only provides trial solutions. Indeed, the admissibility conditions (24) have to be fulfilled in order to define a solution of (22).
The simplest solitary waves cross the threshold only two times, at $\xi_0 = 0$ and at $\xi_1 < 0$, which gives two nonlinear equations

$$\left\{\begin{array}{l} \varphi(0) = -\beta, \\ \varphi(\xi_1) = -\beta. \end{array}\right. \tag{26}$$

The crossing points of the two level curves (26) in the plane (c, ξ_1) determine the speed and the width of trial solutions. We numerically compute the two level curves using a grid with mesh size 0.001. A Gauss-Konrod quadrature formula in a truncated interval $[-10^6, 10^6]$ is used to

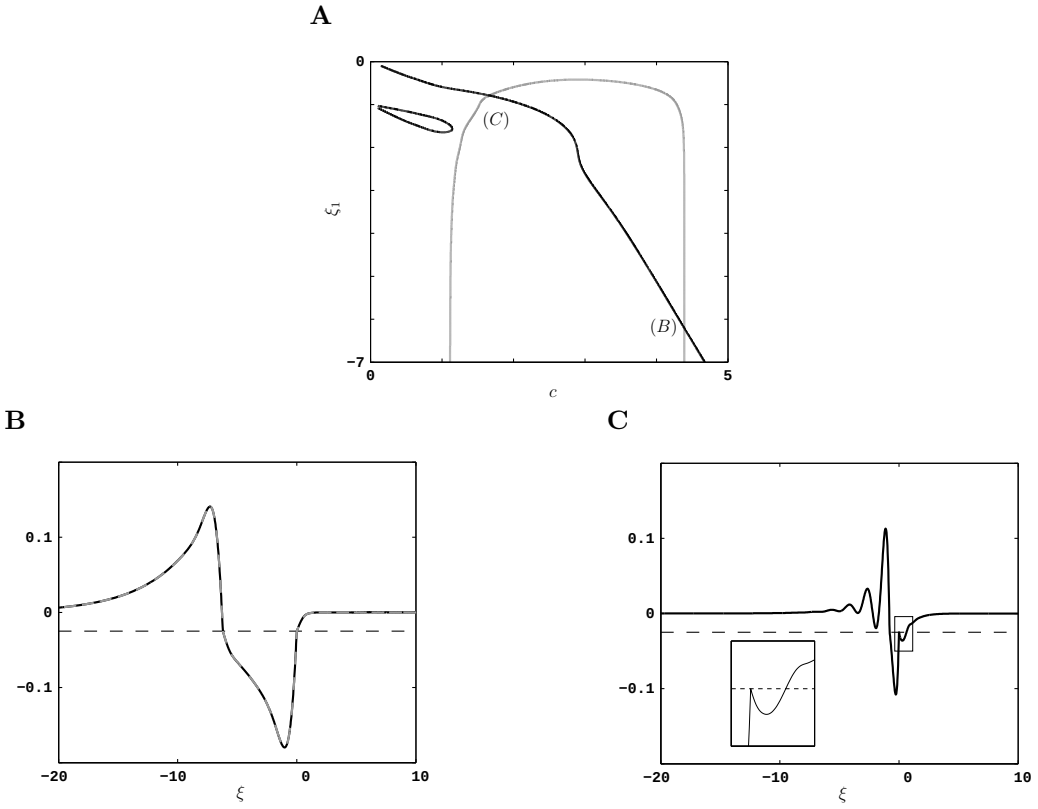

Fig. 11 – In **A** plot of the two level curves $\varphi(\xi_1) = -\beta$ (black) and $\varphi(0) = -\beta$ (grey) in the (c, ξ_1) parameter plane. Crossing points define trial solutions for solitary waves of the Burridge-Knopoff model. The crossing point $(B) \approx (4.39, -6.21)$ is associated with the waveform shown in **B** (black line). We also plot the solution obtained by the numerical simulation of the network (grey dashed). A perfect match is realized with the analytical solution. The crossing point $(C) \approx (1.65, -0.8)$ defines a spurious solution as shown in **C** where the enlargement (inset) reveals the violation of the inequality constraints. Parameters are $k = 2$, $V = 1.025$.

evaluate (25). Approximate solutions for (26) are found with a trust-region dogleg algorithm. As shown in Fig. 11A different crossing points exist.

The inequality constraints of the admissibility conditions have to be checked in order to exclude spurious solutions. Plot of the waveform (25) allows to determine if the sign conditions are fulfilled (see Fig. 11B,C). It can be seen that one of the two crossing points is not associated to a travelling wave solution (see the enlargement in Fig. 11C).

In Fig. 12, we plot the (c, k) curve of the travelling wave solutions. The speed curve is U-shaped with a fold at (c^*, k^*). For $c > c^*$ stable solitary wave solutions are obtained. For $c < c^*$ solitary wave solutions are conjectured to be unstable (they are not observed in the simulations of the network) and become spurious solutions as k increases. A border collision bifurcation is reached below which no solution to (22) can be found with exactly two threshold crossings. We suspect that a travelling sliding solution appears or an additional threshold crossing occurs (both situations are not captured by the present analysis).

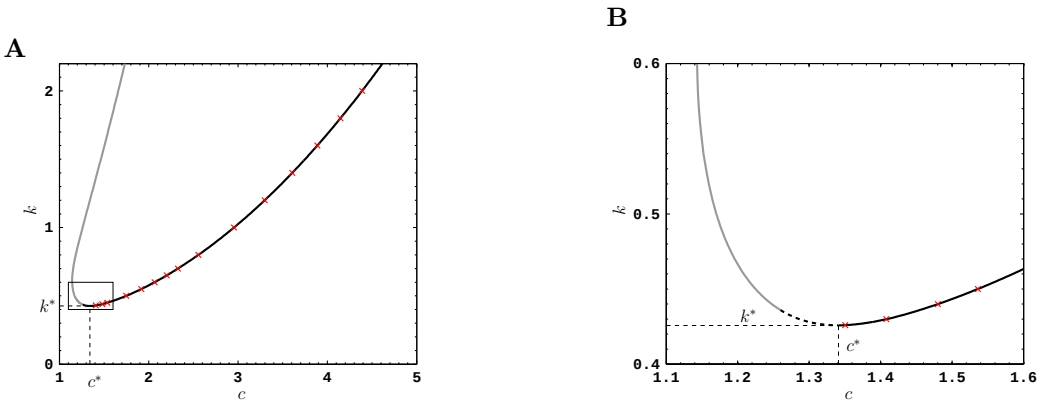

Fig. 12 – **A** and **B** (zoom), curves of the coupling strength k with respect to the wave speed c obtained by solving the non linear system (26). k^* is the critical coupling where propagation failure occurs and c^* is the related wave speed. The full line corresponds to stable solitary wave solutions. The dotted line represents solitary waves that are conjectured to be unstable (not observed in dynamical simulations). The grey line denotes spurious solutions. The red crosses are obtained from network simulations. The fold of the speed curve is located at $c^* \approx 1.34135$, $k^* \approx 0.42585$. As k increases, the solitary waves with $c < c^*$ disappear through a border collision bifurcation at $(c_s, k_s) \approx (1.2598, 0.4360)$. Parameter $V = 1.025$.

5 Discussion

In this paper, we have reported the existence of solitary waves and oscillatory patterns in the excitable Burridge-Knopoff model. We have studied the influence of the friction law and parameters on the robustness and qualitative properties of solitary waves. Wave profiles have been obtained analytically for a piecewise-linear caricature of the friction law. In that case, we have shown that two branches of solitary waves coexist: one corresponding to stable waves whereas the other consists of presumably unstable waves or spurious solutions.

Despite the very different nature of the coupling, the waves observed in the excitable BK model share many similarities with the *taxi waves* recently reported in excitable systems with cross-diffusion [7, 47, 46]. In particular, reflection from boundaries and penetration of solitary waves through each other are observed in both cases, and annihilation of two solitary waves can be also observed in the discrete BK model (results not shown).

A key problem left open in this paper concerns the theoretical justification of the trial solutions (25)-(26), which requires to check the inequality constraints in (24). This problem will be addressed in a next paper in the small coupling limit.

References

[1] V. Acary and B. Brogliato. Numerical methods for nonsmooth dynamical systems. Applications in mechanics and electronics. Springer, 2008.

[2] W. Atkinson and N. Cabrera. Motion of a Frenkel-Kontorova dislocation in a one-dimensional crystal. Phys. Rev. A, 138:763â766, 1965.

[3] Y. Bar-Sinai, R. Spatschek, E. A. Brener, and E. Bouchbinder. Instabilities at frictional interfaces: Creep patches, nucleation, and rupture fronts. Phys. Rev. E, 88:060403, 2013.

[4] Y. Bar-Sinai, R. Spatschek, E. A. Brener, and E. Bouchbinder. On the velocity-strengthening behaviour of dry friction. J. Geophys. Res. Solid Earth, 119:1738â1748, 2014.

[5] Y. Bar-Sinai, R. Spatschek, E. A. Brener, and E. Bouchbinder. Velocity-strengthening friction significantly affects interfacial dynamics, strength and dissipation. Sci. Rep., 5:7841, 2015.

[6] J. Bastien and C. Lamarque. Theoretical study of a chain sliding on a fixed support. Mathematical Problems in Engineering, 2009:19 pages, 2009.

[7] V. N. Biktashev and M. A. Tsyganov. Solitary waves in excitable systems with cross-diffusion. Proc. R. Soc. A, 461:3711–3730, 2005.

[8] E. Bouchbinder, E. A. Brener, I. Barel, and M. Urbakh. Slow cracklike dynamics at the onset of frictional sliding. Phys. Rev. Lett., 107:235501, 2011.

[9] R. Burridge and L. Knopoff. Model and theoretical seismicity. Bull. Seismol. Soc. Am., 57:341–371, 1967.

[10] J. W. Cahn, J. Mallet-Paret, and E. S. Van Vleck. Traveling wave solutions for systems of ODEs on a two-dimensional spatial lattice. SIAM J. Appl. Math., 59:455–493, 1999.

[11] J. M. Carlson and J. S. Langer. Mechanical model of an earthquake fault. Phys. Rev. A, 40:6470–6484, 1989.

[12] J. M. Carlson and J. S. Langer. Properties of earthquakes generated by fault dynamics. Phys. Rev. Lett., 62:2632, 1989.

[13] J. H. E. Cartwright, V. M. Eguíluz, E. Hernández-García, and O. Piro. Dynamics of elastic excitable media. Int J. Bif. Chaos, 9:2197–2202, 1999.

[14] J. H. E. Cartwright, E. Hernández-García, and O. Piro. Burridge-Knopoff models as elastic excitable media. Phys. Rev. Lett., 79:527–530, 1997.

[15] J. C. Comte, P. Tchofo-Dinda, and M. Remoissenet. Discrete Burridge-Knopoff model, with exact solitonic or compactlike traveling wave solution. Phys. Rev. E, 65:026615, 2002.

[16] C. E. Elmer and E. S. Van Vleck. Spatially discrete FitzHugh-Nagumo equations. SIAM J. Appl. Math., 65:1153–1174, 2005.

[17] B. Erickson, B. Birnir, and D. Lavallée. Periodicity, chaos and localization in a Burridgeâ-Knopoff model of an earthquake with rate-and-state friction. Geophys. J. Int., 187:178â198, 2011.

[18] G. B. Ermentrout and D. H. Terman. Mathematical foundations of neuroscience. Springer, 2010.

[19] P. Español. Propagative slipping modes in a spring-block model. Phys. Rev. E, 50:227–235, 1994.

[20] Y. Estrin and Y. Bréchet. On a model of frictional sliding. Pure Appl. Geophys., 147:745–762, 1996.

[21] M. Feingold, D. L. Gonzalez, O. Piro, and H. Viturro. Phase locking, period doubling, and chaotic phenomena in externally driven excitable systems. Phys. Rev. A, 37:4060–4063, 1988.

[22] R. FitzHugh. Impulses and physiological states in theoretical models of nerve membrane. Biophysical Journal, 1:445 – 466, 1961.

[23] N. Flytzanis, S. Crowley, and V. Celli. High velocity dislocation motion and interatomic force law. J. Phys. Chem. Solids, 38:539–552, 1976.

[24] J. P. Gong. Friction and lubrication of hydrogels - its richness and complexity. The Royal Society of Chemistry 2006, 2:544–552, 2006.

[25] H. P. McKean Jr. Nagumo's equation. Adv. Math., 4:209–223, 1970.

[26] F. Heslot, T. Baumberger, B. Perrin, C. Caroli, and B. Caroli. Creep, stick-slip, and dry friction dynamics: Experiments and a heuristic model. Phys. Rev. E, 49:4973–4988, 1994.

[27] W. Huang and X. Wang. Biomimetic design of elastomer surface pattern for friction control under wet conditions. Bioinspiration and Biomimetics, 8:046001, 2013.

[28] H. J. Hupkes and B. Sandstede. Travelling pulses for the discrete FitzHugh-Nagumo system. SIAM J. Appl. Dyn. Syst., 9:827–882, 2010.

[29] E. M. Izhikevich. Dynamical systems in neuroscience: The geometry of excitability and bursting. The MIT Press, 2007.

[30] Y. Y. Kagan. Observational evidence for earthquakes as a nonlinear dynamic process. Physica D, 77:160–192, 1994.

[31] B. Kaproth and C. Marone. Slow earthquakes, preseismic velocity changes, and the origin of slow frictional stick-slip. Science, 341:1229â1232, 2013.

[32] J. P. Keener. Propagation and its failure in coupled systems of discrete excitable cells. SIAM J. Appl. Math., 47:556–572, 1987.

[33] M. Lebellego. Phénomènes ondulatoires dans un modèle discret de faille sismique. PhD thesis, Université de Toulouse, 2011.

[34] C. B. Muratov. Traveling wave solutions in the Burridge-Knopoff model. Phys. Rev. E, 59:3847–3857, 1999.

[35] A. Ohmura and H. Kawamura. Rate- and state-dependent friction law and statistical properties of earthquakes. EPL (Europhysics Letters), 77:69001, 2007.

[36] T. Putelat, J. Dawes, and J. Willis. Regimes of frictional sliding of a spring-block system. J. Mech. Phys. Sol., 58:27–53, 2010.

[37] M. Remoissenet. Waves called solitons - Concepts and experiments. Springer Verlag Berlin, 1999.

[38] J. Rinzel and J. B. Keller. Traveling wave solutions of a nerve conduction equation. Biophys. J., 13:1313–1337, 1973.

[39] J. Schmittbuhl, J. P. Vilotte, and S. Roux. Propagative macrodislocation modes in an earthquake fault model. Europhys. Lett., 21:375–380, 1993.

[40] J. Schmittbuhl, J. P. Vilotte, and S. Roux. A dissipation-based analysis of an earthquake fault model. J. Geophys. Res., 101:27741–27764, 1996.

[41] C. Scholz. The Mechanics of Earthquakes and Faulting. Cambridge University Press, 2002.

[42] H. Schwetlick and J. Zimmer. Existence of dynamic phase transitions in a one-dimensional lattice model with piecewise quadratic interaction potential. SIAM J. Math. Anal., 41:1231–1271, 2009.

[43] T. Shimamoto. Transition between frictional slip and ductile flow for halite shear zones at room temperature. Science, 231:711–714, 1986.

[44] A. Tonnelier. McKean caricature of the FitzHugh-Nagumo model: traveling pulses in a discrete diffusive medium. Phys. Rev. E, 67:036105, 2003.

[45] L. Truskinovsky and A. Vainchtein. Kinetics of martensitic phase transitions: Lattice model. SIAM J. Appl. Math., 66:533–553, 2005.

[46] M. A. Tsyganov and V. N. Biktashev. Classification of wave regimes in excitable systems with linear cross-diffusion. Phys. Rev. E, 90:062912, 2014.

[47] M. A. Tsyganov, V. N. Biktashev, J. Brindley, A. V. Holden, and G. R. Ivanitsky. Waves in systems with cross-diffusion as a new class of nonlinear waves. Physics-Uspekhi, 50:263–286, 2007.

[48] N. A. Venturi and F. Nori. Marginal stability and chaos in coupled faults modelled by nonlinear circuits. Phys. Rev. Lett., 74:74–77, 1995.

[49] K. Vorvolakos and M. K. Chaudhury. The effects of molecular weight and temperature on the kinetic friction of silicone rubbers. Langmuir, 19:6778–6787, 2003.

[50] J. Wang. One-dimensional dynamical modelling of earthquakes: a review. Terr. Atmos. Ocean. Sci, 19:183–203, 2008.

[51] J. Wang and R. Hwang. One-dimensional dynamic simulations of slip complexity of earthquake faults. Earth Planets Space, 53:91–100, 2001.

[52] F. Wu-Bavouzet, J. Clain-Burckbuchler, A. Buguin, P.-G. De Gennes, and F. Brochard-Wyart. Stick-Slip: wet versus dry. The Journal of Adhesion, 83:761–784, 2007.

[53] X. Xiong, R. Kikuuwe, and M. Yamamoto. Implicit Euler simulation of one-dimensional Burridge-Knopoff model of earthquakes with set-valued friction laws. Advances in Computational Mathematics, 41:1039–1057, 2015.

[54] H. J. Xu and L. Knopoff. Periodicity and chaos in a one-dimensional dynamical model of earthquakes. Phys. Rev. E, 50:3577–3581, 1994.

[55] E. C. Zeeman. Differential equations for the heartbeat and nerve impulse. In Towards a theoretical biology, volume 4, pages 8–67. Edinburgh University Press Edinburgh, 1972.

[56] E. P. Zemskov, E. P. Zykov, V. S. Kassner, and S. C. Muller. Stability of travelling fronts in a piecewise-linear reaction-diffusion system. Nonlinearity, 13:2063–2076, 2000.

Contents

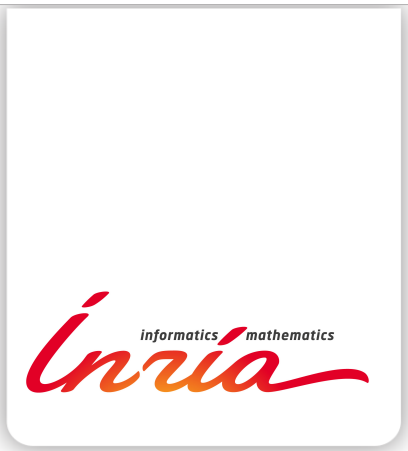

RESEARCH CENTRE
GRENOBLE – RHÔNE-ALPES

Inovallée
655 avenue de l'Europe Montbonnot
38334 Saint Ismier Cedex

Publisher
Inria
Domaine de Voluceau - Rocquencourt
BP 105 - 78153 Le Chesnay Cedex
inria.fr

ISSN 0249-6399